JTTEE5 11:400–408
© ASM International

Peer Reviewed

Microstructure and Stresses in HVOF Sprayed Iron Aluminide Coatings

T.C. Totemeier, R.N. Wright, and W.D. Swank

(Submitted 31 January 2001; in revised form 30 March 2001)

The microstructure and state of stress present in Fe_3Al coatings produced by high velocity oxygen fuel (HVOF) thermal spraying in air at varying particle velocities were characterized using metallography, curvature measurements, x-ray analysis, and microhardness measurements. Sound coatings were produced for all conditions. The microstructures of coatings prepared at higher velocities showed fewer unmelted particles and a greater extent of deformation. Residual stresses in the coatings were compressive and varied from nearly zero at the lowest velocity to approximately −450 MPa at the highest velocity. X-ray line broadening analyses revealed a corresponding increase in the extent of cold work present in the coating, which was also reflected in increased microhardness. Values of mean coefficient of thermal expansion obtained for as-sprayed coatings using x-ray analysis were significantly lower than those for powder and bulk alloy.

Keywords coatings, HVOF, iron aluminide, residual stress, thermal expansion, x-ray diffraction

1. Introduction

Alloys based on the iron aluminide intermetallic Fe_3Al have been recently developed as potential replacement materials for stainless steels in applications requiring high-temperature oxidation and sulfidation resistance, such as heating elements, furnace fixtures, and piping for fossil energy applications.[1-3] The excellent resistance of Fe_3Al-based alloys to these conditions has been well documented.[4,5] Their use, however, has been limited by relatively low room-temperature ductility, and poor strength and creep resistance above 600 °C.[2] Both of these problems can be alleviated to a degree by appropriate alloying additions, but it has proven difficult to formulate an alloy with both good creep resistance and low-temperature ductility. The use of these alloys as oxidation- and corrosion-resistant coatings on stronger, less-resistant substrate materials holds promise as a means of overcoming their low creep resistance.

Thermal spraying of a Fe_3Al-based alloy has been accomplished using high velocity oxygen fuel (HVOF) spraying and air plasma spraying (APS).[6] Coatings produced using the APS process apparently debonded upon cooling from the deposition temperature, whereas HVOF sprayed coatings on a 1018 carbon steel substrate were well bonded and dense. The HVOF sprayed coatings were in a state of residual compression at room temperature. Coatings produced from a FeAl intermetallic alloy have also been prepared using HVOF spraying.[7] As with the previous study on Fe_3Al, the coatings produced were dense and well bonded to the substrate. A nanocrystalline structure introduced into the starting powders by cyromilling was retained after coating because of the lower particle temperatures achieved in HVOF spraying.

The observation of compressive residual stresses in metallic coatings is characteristic of the HVOF thermal spray process, especially in comparison with plasma spraying, in which tensile residual stresses are typically present. The state of residual stress in a thermally sprayed coating is a combination of intrinsic deposition stresses and thermal mismatch stresses produced on cooling from the deposition temperature. For plasma sprayed coatings, the deposition stresses are tensile, primarily resulting from particle "quench" stresses.[8-10] For the HVOF process, compressive peening stresses resulting from the high-velocity impact of solid or semisolid particles on the substrate appear to be dominant. The impact of hard particles results in constrained local plastic deformation of the underlying material and compressive residual stresses. Recent studies have examined the effect of processing conditions on the state of residual stress in HVOF sprayed stainless steel coatings and have shown that higher kinetic energy particles produce higher compressive stresses.[11]

This article describes the characterization of microstructure and stresses in Fe_3Al coatings produced by HVOF thermal spraying. The nature of the peening stress was examined by studying coatings which had been prepared at three different torch chamber pressures, corresponding to three different particle velocities. Residual stresses in the coatings were characterized by curvature measurement and x-ray diffraction (XRD). Line broadening analysis and coating microhardness measurements were performed to characterize the extent of cold work in the coatings and its effect on strength. XRD was also used to measure thermal expansion coefficients of the coatings in-situ on the substrate.

2. Experimental Procedures

2.1 Coating Preparation

Coatings were produced on type 304 stainless steel substrates using commercially available Fe_3Al alloy (designated FAS)

T.C. Totemeier, R.N. Wright, and **W.D. Swank,** Idaho National Engineering and Environmental Laboratory, Bechtel BWXT Idaho, LLC, P.O. Box 1625, MS 2218, Idaho Falls, ID 83415. Contact e-mail: totetc@inel.gov.

Table 1 Coating Parameters, Particle Characteristics, and Thicknesses

Chamber Pressure, kPa	Equivalence Ratio	Average Particle Temperature, °C	Average Particle Velocity, m/s
170	1.0	1450	390
340	1.0	1750	570
620	1.0	1600	630

powder with nominal composition Fe-28%Al-2%Cr (at.%). The powder was obtained from Ametek Specialty Metal Products (Eighty Four, PA) with a size distribution such that essentially all of the particles were less than 38 μm in diameter (−270 mesh). The substrates were rectangular strips 76 × 12.5 × 1.6 mm in size and were grit blasted with Al_2O_3 particles prior to spraying. Both sides of the substrates were grit blasted so that the strips were nominally flat prior to coating application.

HVOF spraying was performed in air at an atmospheric pressure of 85.5 kPa using a model JP-5000 system (Hobart-Tafa Technologies, Concord, NH). The coatings were built up layer by layer using a raster deposition scheme. At a transverse velocity of 200 mm/s and a standoff distance of 355 mm, each pass of the substrate in front of the torch adds an approximately 45 μm thick layer. The substrates were free to bend in response to thermal and coating stresses, and were air cooled from behind during spraying. Detailed descriptions of the spray system and gas flow field characteristics are given in Ref. 12.

Coatings were produced at an equivalence ratio of 1 (a stoichiometric mixture of kerosene and oxygen) and three torch chamber gauge pressures: 170, 340, and 620 kPa. The particle temperature and velocity characteristics for each condition were measured using an integrated laser Doppler velocimeter and high speed two-color pyrometer.[12,13] The estimated (1σ) measurement uncertainties are 5% for particle temperature (assuming gray body behavior) and less than 5 m/s for particle velocity. Well-bonded, dense coatings approximately 300 μm thick were obtained; Table 1 lists the relevant coating parameters, particle velocities, and temperatures. It is apparent that increasing chamber pressure results in higher average particle velocities, in agreement with observations for Inconel 718 powders reported in Ref. 13. The sprayed particle temperature is a function of the flame temperature and particle residence time in the flame. Because the chamber pressure increases both the flame length and the particle velocity, these competing effects result in the particle temperature being a complex function of chamber pressure, as indicated in Table 1.

2.2 Characterization Techniques

2.2.1 Optical Microscopy and Microhardness. The microstructural features of the coatings were examined in the as-sprayed condition and after annealing for approximately 1 h at 800 °C (incurred during thermal expansion testing described below) using standard metallographic techniques. The coatings were examined in the as-polished condition and after etching in aqua regia (75 vol.% HNO_3, 25 vol.% HCl). Vickers microhardness measurements were made on the polished sections using a 300 g load; five indentations were made at the coating midplane for both conditions.

2.2.2 Curvature Measurements. Net residual stresses in the as-sprayed coatings were estimated from curvature measurements of the coating-substrate couples made using an optical comparator. Stresses were calculated from curvature using assumptions of linear elastic behavior and biaxial in-plane coating stresses, which result in the following equation[14,15]:

$$\sigma_c = \overline{E}_c(\varepsilon_0 - \varepsilon) + \overline{E}_c(x - t_n)\kappa \quad \text{(Eq 1)}$$

where σ_c is the in-plane stress in the coating, $\overline{E}_c$ is the coating biaxial modulus (equal to E_c divided by $1 - \nu$), κ is the curvature (inverse radius of curvature), x is the position within the coating ($x = 0$ at the coating-substrate interface and $x = t_c$ is the coating surface, where t_c is coating thickness), and

$$t_n = \frac{\overline{E}_c t_c^2 - \overline{E}_s t_s^2}{2(\overline{E}_c t_c + \overline{E}_s t_s)} \quad \text{(Eq 2)}$$

$$\varepsilon = \frac{\kappa[\overline{E}_s^2 t_s^4 + \overline{E}_c^2 t_c^4 + 2\overline{E}_s\overline{E}_c t_s t_c(2t_s^2 + 2t_c^2 + 3t_s t_c)]}{6\overline{E}_s\overline{E}_c t_s t_c(t_s + t_c)} \quad \text{(Eq 3)}$$

$$\varepsilon_0 = \frac{\varepsilon\overline{E}_c t_c}{\overline{E}_s t_s + \overline{E}_c t_c} \quad \text{(Eq 4)}$$

where $\overline{E}_s$ is the substrate biaxial modulus and t_s is the substrate thickness. For 316 stainless steel, a value of 276 GPa was used for $\overline{E}_s$ (based on Young's modulus of 193 GPa and Poisson's ratio of 0.3[16]), and for Fe_3Al a value of 201 GPa was used for $\overline{E}_c$ (based on Young's modulus of 141 GPa and Poisson's ratio of 0.3[17]). The surface stress ($x = t_c$), the interface stress ($x = 0$), and the coating average stress ($x = t_c/2$) were calculated using this method.

2.2.3 X-Ray Diffraction. XRD was used to characterize the residual stress and the degree of cold work in the coatings, and also to measure the coefficient of thermal expansion (CTE) of the coating in-situ on the substrate. Residual stresses were measured using the two-tilt method, the degree of cold work was assessed with line broadening analysis using the Warren-Averbach method,[18] and CTE was measured from peak shifts with increasing temperature. All x-ray measurements were made on a AXS theta-theta diffractometer (Bruker, Madison, WI), using Cu-Kα radiation produced at a tube voltage of 40 kV. A Göbels mirror attachment was used to provide a parallel incident beam, and a LiF monochromator was used to filter fluorescent radiation. The depth of penetration for Cu-Kα radiation in Fe_3Al for the (211) B2 peak ($2\theta = 81°$) is approximately 5 μm, calculated using a mass-fraction weighted average of adsorption coefficients for Fe and Al.

Two different surface conditions were examined. As-sprayed surfaces were analyzed using the line broadening method. Residual stress, line broadening, and CTE measurements were made on samples for which the coating surface was polished and etched. Polishing of the surfaces was performed to provide better diffracted signal strength and to obtain stress measurements without the effects of the as-sprayed surface roughness. Because the polishing procedure could potentially affect the stress state of the coating, care was taken to minimize the extent of mechanical damage. Initial polishing was performed using a 6

μm diamond paste, followed by 3 μm diamond paste and final polishing using a 0.3 μm alumina slurry. After they were polished, the coating surfaces were strongly etched in aqua regia to remove any damaged layers. Line broadening analysis of an annealed sample before and after the polishing procedure revealed no effect, and the consistency of line broadening analysis results (described below) for as-sprayed and polished samples also indicated the lack of an effect of polishing.

The two-tilt measurement was performed to provide an indication of the magnitude of residual stresses present in the coating and any trends with varying particle velocity, and for comparison with the curvature measurements. This measurement is a simplified version of the $\sin^2\psi$ method.[19] Measurements were made in the longitudinal direction of the coating on a (220) B2 peak (approximately 97° 2θ) at tilts (angle ψ) of 0° and 35°. A Pearson VII function was fitted to the measured line profiles to determine the precise peak positions. Residual stresses were calculated using the equation

$$\sigma = \frac{E}{(1+\nu)\sin^2\psi}\left(\frac{d_i - d_n}{d_n}\right) \quad \text{(Eq 5)}$$

where E is the elastic modulus, ν is Poisson's ratio (taken as 0.3), and d_n and d_i are the spacings of (220) planes measured at tilts of 0° and 35°, respectively.

It was recognized that the relatively low-angle peak and low $\sin^2\psi$ values used lead to less precise values than typical for residual stress measurements, but the accuracy obtained was deemed adequate for the purposes described above. Following the analysis outlined in Ref. 20, the error in stress due to an assumed 0.01° error in peak position was calculated to be 25 MPa.

Line broadening analysis provides a measurement of the degree of cold work present in terms of the size and distribution of coherently diffracting domains within the coating and the magnitude of microstrain present. The profiles of the (110) and (220) peaks (referenced to the B2 lattice) at 44° and 97° 2θ were measured for analysis. The gas-atomized Fe_3Al powder from which the coatings were prepared was used as the strain-free standard. Analysis using the Warren-Averbach method[18] was performed using the Bruker Crysize program following peak fitting with split Pseudo-Voigt functions. The dislocation density, ρ, for each condition was computed using the following relationship[21]:

$$\rho = \frac{2\sqrt{3}\langle\varepsilon^2\rangle^{1/2}}{|\vec{b}|\,D} \quad \text{(Eq 6)}$$

where the term $\langle\varepsilon^2\rangle^{1/2}$ is the root mean square (RMS) microstrain, $\vec{b}$ is the Burger's vector, and D is the average column length. For the Fe_3Al coatings, the partial B2 dislocation Burger's vector was used [magnitude $(3^{1/2}/2)a$, where a is lattice parameter].

The thermal expansion coefficients of the coatings were determined by measuring the shift in position of the (211) peak with increasing temperature. Measurements were performed using a high-temperature stage at temperatures of 25, 200, 400, 600, and 800 °C. Each measurement took approximately 1 h. The measurement at room temperature was repeated after the heating cycle; the difference in peak position before and after heating was used to estimate the residual stress relieved during the heating cycle. Precise peak positions were obtained by fitting raw data with Pearson VII functions.

3. Results

3.1 Coating Microstructure and Microhardness

Figure 1 shows representative etched microstructures of coatings produced at the three particle velocities, and Table 2 lists quantitative microstructural features. All coatings show a dense structure with good conformity and little resolvable porosity, being composed of a mixture of unmelted particles (light, roughly hemispherical shapes) and melted particles, which solidified as the coating formed (darker regions). At a velocity of 390 m/s, there is a relatively large fraction (40 vol.%) of unmelted particles, which have fairly circular shapes (mean aspect ratio of 1.5). There is also a qualitatively greater amount of porosity than in coatings produced at higher particle velocities. Although there is only a slightly smaller fraction of unmelted particles in the coating produced at 570 m/s (35 vol.%), they appear more deformed with a slightly higher mean aspect ratio (1.8). At the highest particle velocity (630 m/s), the volume fraction of unmelted particles is significantly reduced (to 20 vol.%), and the particles present are severely deformed, with a mean aspect ratio of 2.4. In addition, the density of oxide stringers is higher in the 630 m/s coating relative to the 390 m/s coating, indicating that more compression of the coating features has occurred.

No significant changes in coating microstructure occurred as a result of polishing and heating to 800 °C during the CTE measurement process. Figure 2 shows representative microstructures of polished and annealed coatings. In particular, the grain size observable in the unmelted particles (approximately 10-20 μm) has not increased.

Table 3 lists Vickers hardness numbers (VHN) for the three coatings in the as-sprayed condition and after 1 h at 800 °C. Also shown are corresponding yield stresses calculated using the formula[22]

$$\sigma_0 = \frac{\mathrm{VHN}}{3}(0.1)^n \quad \text{(Eq 7)}$$

where σ_0 is the yield stress and n is the strain-hardening coefficient, taken as 0.15 for the work-hardened coatings.[23] The hardness of the coatings increases with increasing particle velocity, from 314 kg/mm^2 at 390 m/s to 515 kg/mm^2 at 630 m/s. Annealing at 800 °C for approximately 1 h somewhat reduces the hardness of all coatings, but not dramatically. The hardnesses after 800 °C exposure still increase with particle velocity. The corresponding yield stresses are relatively high compared with typical values for wrought Fe_3Al (see Discussion). The minimum value, for the 390 m/s coating after 800 °C exposure, was 610 MPa, and the maximum, for the as-sprayed 630 m/s coating, was nearly 1200 MPa.

3.2 Residual Stresses

3.2.1 Curvature. All samples exhibited a positive curvature, i.e., the coated surface assumed a convex shape, indicating a compressive residual stress in the coating. Curvature measurements for coatings sprayed at the three different velocities are

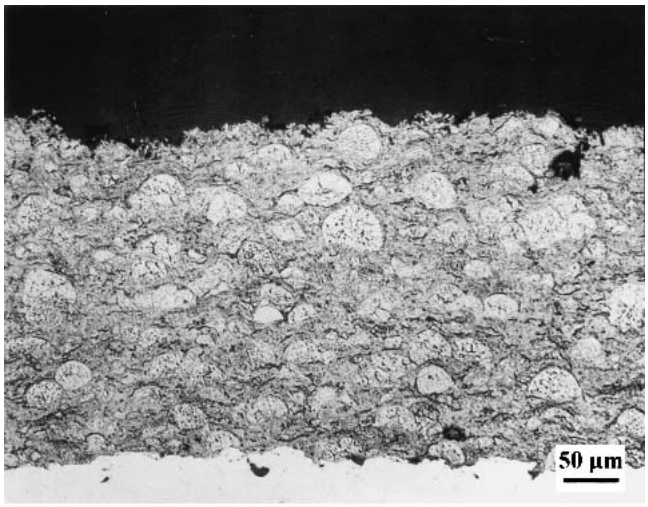

(a)

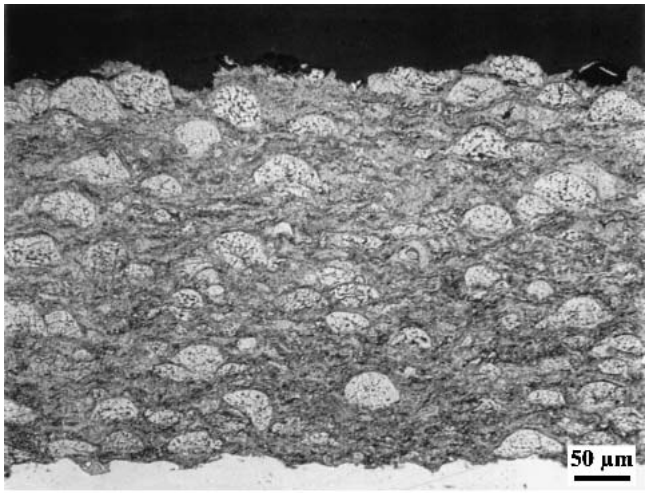

(b)

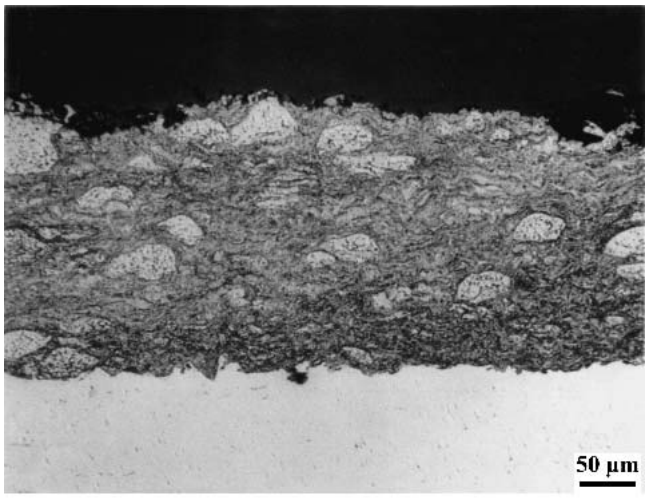

(c)

Fig. 1 Representative microstructures (200×) of coatings sprayed at **(a)** 390 m/s, **(b)** 570 m/s, and **(c)** 630 m/s

Table 2 Coating Microstructural Features

Particle Velocity, m/s	As-Sprayed Thickness, µm	Polished Thickness, µm	Unmelted Particles, vol. %	Mean Aspect Ratio of Unmelted Particles
390	300	200	40	1.5
570	340	230	35	1.8
630	240	140	20	2.4

listed in Table 4, along with calculated residual stresses at the coating surface, the coating-substrate interface, and the coating midplane (average stress). The magnitude of residual stress increases with increasing particle velocity, from approximately −100 MPa at a velocity of 390 m/s, to more than −400 MPa at a velocity of 630 m/s. For comparison, the coating stresses that would have developed on a thick, nondeformable substrate were also calculated from the measured curvature. The curvature was used to calculate the coating-substrate mismatch strain $\Delta\varepsilon$, as defined in Ref. 8. Assuming that the strain was completely accommodated in the coating, the resulting coating stress was calculated as $\Delta\varepsilon\overline{E}_c$. Values for the three particle velocities are −160 MPa for 390 m/s, −380 MPa for 570 m/s, and −810 MPa for 630 m/s.

3.2.2 X-Ray Measurement. Table 5 lists measured peak positions, corresponding *d*-spacings, and calculated residual stresses for polished and etched coatings produced at each particle velocity. The residual stresses become increasingly compressive with increasing velocity. The value for the coating sprayed at 390 m/s, a tensile stress of 32 MPa, can be taken as essentially zero, because the approximate error in the stress measurement is ± 25 MPa.

3.3 Crystallite Size and Microstrain

Table 6 lists results of the line broadening analysis. As mentioned above, the column lengths, microstrains, and dislocation densities are similar for the as-sprayed and polished surface conditions, indicating little effect of polishing on the state of surface stress. This observation is also supported by the lack of increase in dislocation density for the 630 m/s coating, which was repolished after annealing.

The average column lengths and microstrains for the as-sprayed coatings sprayed at the two lower velocities (390 and 570 m/s) are essentially equal. The column lengths for these coatings (which roughly correspond to subgrain size) are greater than that for the coating sprayed at 630 m/s, whereas the degree of microstrain in the higher velocity coating is greater than in the lower velocity coatings. The differences correspond to a doubling in the dislocation density for the coating formed at 630 m/s in comparison to the lower velocities.

As expected, annealing at 800 °C for an hour significantly reduces the degree of cold work present in the coatings. The dislocation density is reduced by approximately a factor of 5 for the low velocity coatings, and by an order of magnitude for the highest velocity coating.

3.4 Thermal Expansion

Figure 3 is a plot of thermal expansion data for FAS powder and the three coatings. Literature data for bulk Fe_3Al[17] is also

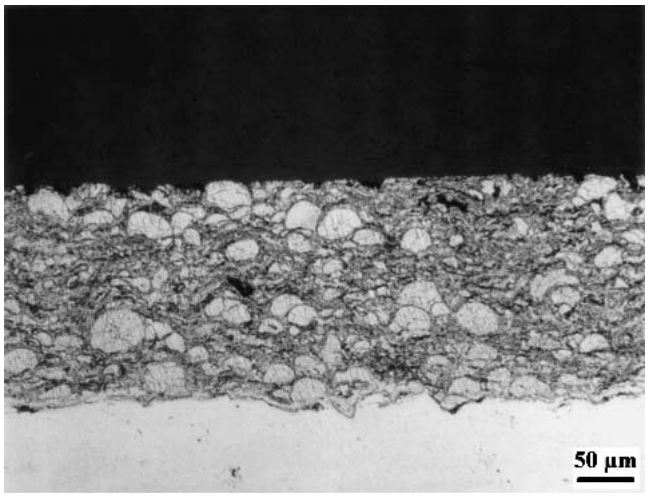

(a)

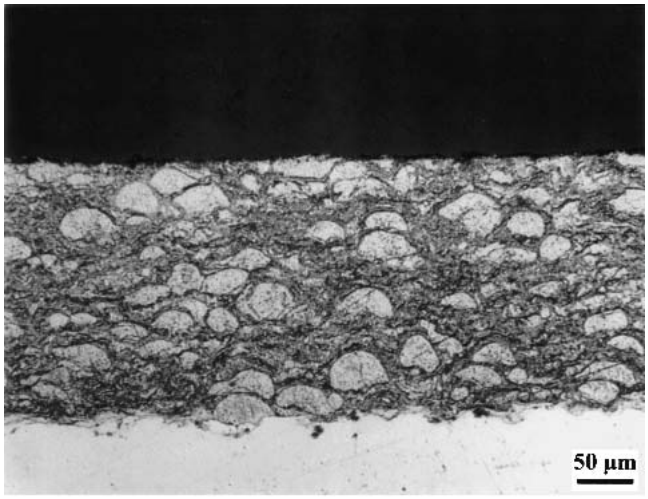

(b)

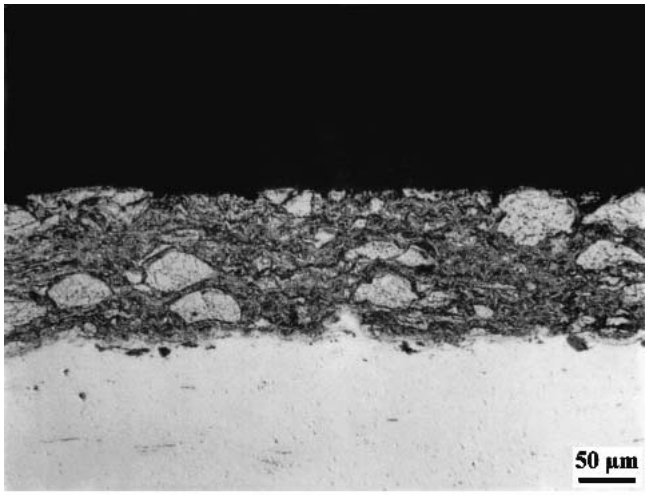

(c)

Fig. 2 Representative microstructures (200×) of coatings at **(a)** 390 m/s, **(b)** 570 m/s, and **(c)** 630 m/s after surface polishing and heating for 1 h at 800 °C

Table 3 Vickers Microhardness (300 g Load) and Corresponding Yield Stress

Particle Velocity, m/s	Condition	Vickers Hardness Number, kg/mm^2 Range	Vickers Hardness Number, kg/mm^2 Mean	Corresponding Yield Stress, MPa
390	As-sprayed	254-355	314	720
390	Polished, 1 h at 800 °C	222-304	266	610
570	As-sprayed	358-434	394	900
570	Polished, 1 h at 800 °C	357-388	369	840
630	As-sprayed	464-555	515	1180
630	Polished, 1 h at 800 °C	372-445	409	940

Table 4 Coating Residual Stresses Calculated From Curvature

Particle Velocity, m/s	Coating Thickness, µm	Curvature, m^{-1}	Surface Stress, MPa	Interface Stress, MPa	Average Stress, MPa
390	280	0.31	−90	−105	−95
570	400	0.89	−140	−210	−175
630	330	1.70	−370	−485	−430

Table 5 Two-Tilt X-Ray Residual Stress Measurements

Particle Velocity, m/s	Tilt Angle, ψ, °	Peak Position, 2θ, °	Plane Spacing, d_{220}, Å	Residual Stress, σ, MPa
390	0	97.388	1.0254	
	35	97.375	1.0255	+32
570	0	97.268	1.0264	
	35	97.365	1.0256	−244
630	0	97.167	1.0272	
	35	97.354	1.0257	−473

Table 6 Line Broadening Analysis Results

Particle Velocity, m/s	Condition	Average Column Length, Å	RMS Microstrain, 50 Å Column	Dislocation Density, cm^{-2}
390	As-sprayed	293	3.1×10^{-3}	1.5×10^{11}
390	Polished and etched	243	3.1×10^{-3}	1.8×10^{11}
390	Polished, 1 h at 800 °C	681	1.5×10^{-3}	3.0×10^{10}
570	As-sprayed	306	3.6×10^{-3}	1.6×10^{11}
570	Polished and etched	233	4.3×10^{-3}	2.5×10^{11}
570	Polished, 1 h at 800 °C	420	1.3×10^{-3}	4.4×10^{10}
630	As-sprayed	196	4.6×10^{-3}	3.2×10^{11}
630	Polished and etched	172	4.7×10^{-3}	3.8×10^{11}
630	Polished, 1 h at 800 °C	504	1.7×10^{-3}	4.6×10^{10}
630	Repolished after 800 °C	264	5.0×10^{-5}	2.6×10^{9}

plotted for comparison. The powder data closely mirror the literature values, whereas the data for the coatings are consistently lower and show a large scatter. At the two highest temperatures (600 and 800 °C), there is a trend in mean CTE as a function of particle velocity, with the coating sprayed at the lowest velocity

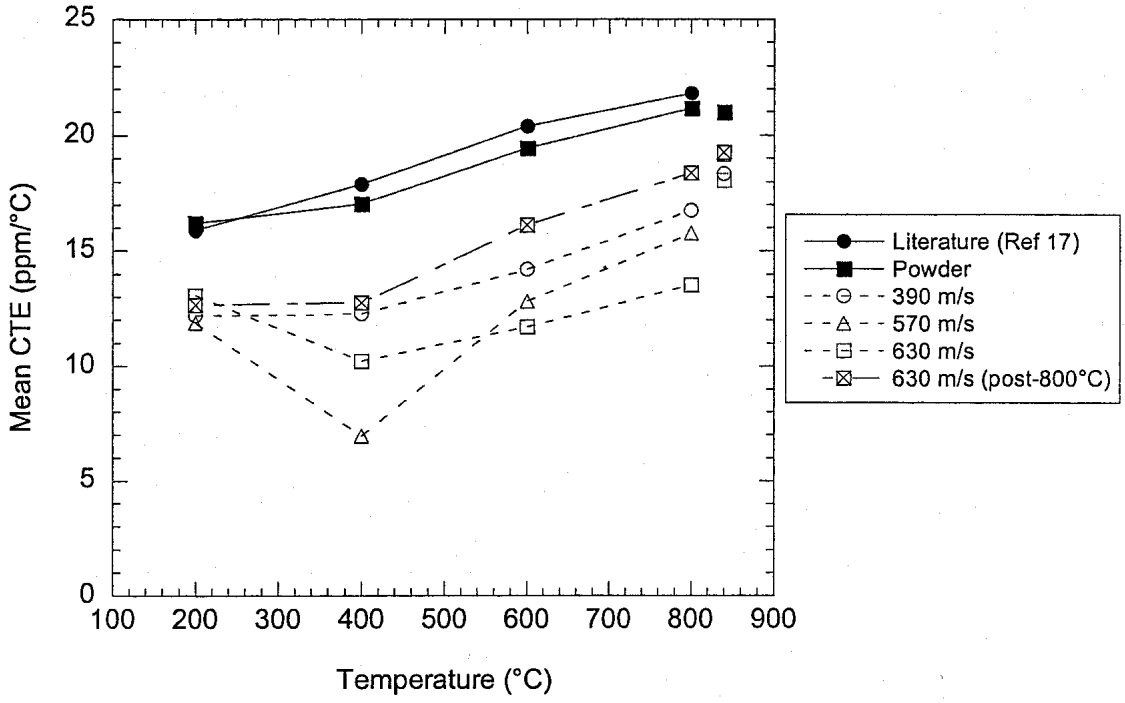

Fig. 3 Mean CTE versus temperature for Fe_3Al coatings and powder. Isolated data points at 840 °C represent mean CTE for cooling from 800-25 °C.

Table 7 Changes in (211) Peak Position Because of Heating to 800 °C in Thermal Expansion Tests, and Corresponding Residual Stresses

Particle Velocity, m/s	As-Sprayed 2θ, °	Post-Heat 2θ, °	$(d_1 - d_2)/d_2$	Residual Stress, MPa
390	81.236	81.355	1.2×10^{-3}	−280
570	81.108	81.363	2.6×10^{-3}	−610
630	81.015	81.356	3.5×10^{-3}	−820

showing the highest CTE. There is no such grouping at lower temperatures. The CTE data for the coatings at 400 °C do not follow the trend of the data at higher and lower temperatures, and are significantly lower. For the 390 and 630 m/s coatings the mean CTE at 400 °C is lower than at 200 °C. Figure 3 includes data for a 630 m/s coating that was measured after one cycle of heating to 800 °C. The mean CTE for this coating is much higher than in the as-sprayed condition, and the difference between the heating and cooling CTE is much smaller.

Also shown in Fig. 3 are the mean CTEs obtained on cooling from 800 °C to room temperature—these data are slightly offset to the right of the other data. The cooling CTE was calculated from the peak position at 800 °C and that obtained at 25 °C after cooling, whereas the heating CTE values were calculated using the position of the 25 °C peak prior to heating. There is no difference between the heating and cooling CTE for the powder, but the cooling CTEs are consistently higher for the coatings.

The position of the (211) peak at room temperature is shifted to higher angles after heating to 800 °C (Table 7). The *d*-spacing changes reflect a decrease in strain through the thickness of the coating, which is likely primarily a result of alleviation of in-plane residual stress due to annealing at 800 °C. The corresponding residual stresses were calculated (assuming a biaxial stress state) using the relation:

$$\sigma = \frac{E}{2\nu}\left(\frac{d_1 - d_2}{d_2}\right) \quad \text{(Eq 8)}$$

where d_1 is the (211) spacing before heating and d_2 is the spacing after heating. The stresses increase with increasing particle velocity, as observed for the two-tilt residual stress and curvature measurements, but the magnitudes are higher in this case. In particular, the shift in spacing due to annealing indicates a significant compressive residual stress for the coating sprayed at 390 m/s, where none was indicated in the two-tilt measurement.

4. Discussion

4.1 Coating Parameters, Microstructure, and Residual Stress

The results obtained in this study indicate a strong effect of HVOF particle velocity on the microstructure and stress state of the coating produced. The effect is seen in the residual stress, degree of cold work, and coating hardness. The residual stresses, measured using three different techniques (curvature, two-tilt x-ray, and peak shift on annealing), vary from nearly zero for the coating produced at 390 m/s to highly compressive (around 400-600 MPa) for the coating produced at 630 m/s. The magnitudes of the residual stresses will increase if the coating is formed on a thick substrate, which does not bend. According to the results of calculations presented in Section 3.2.1, the stresses on thick substrates would range from −160 MPa for a coating formed at 390

m/s to −810 MPa for a coating formed at 630 m/s. Because of the higher stresses, it is possible that a coating successfully applied to a thin substrate may spall when applied to a thick substrate.

The extent of microscopic deformation, as measured in line broadening analysis, also increases with increasing particle velocity, although in this case the differences between the three velocities are somewhat less pronounced. All coatings show relatively high dislocation densities, which increase from 1.5×10^{11} to 3.8×10^{11} cm^{-2} going from the lowest to highest particle velocity. These values are of similar magnitude to those of heavily cold-rolled metals,[24] indicating that extensive deformation has occurred during the coating process for coatings produced at all velocities. Correspondingly high hardness values are observed, which also increase with particle velocity.

The above observations highlight the important role that peening effects play in HVOF spraying of metallic coatings, as originally discussed in Ref. 11. Solid or semisolid particles with higher kinetic energy will produce a greater extent of constrained deformation in the underlying material, hence giving rise to higher compressive residual stresses and a large amount of cold work. The total net residual stress of the coating after spraying is a combination of contributions from compressive peening stress, tensile quench stress, and coating-substrate thermal mismatch stress, which may be tensile or compressive. For the coating produced at 390 m/s, the peening and quench stresses are apparently of similar magnitude, leading to a coating with relatively little net residual stress, but that is still heavily cold-worked. The CTE of the Fe_3Al alloy and the stainless steel substrate are nearly identical, and there is therefore little thermal mismatch stress. For the coatings produced at 570 and 630 m/s, the peening stress is dominant and the net residual stresses are compressive. This interplay enables the state of stress of the coating to be readily manipulated via the particle velocity and tailored to the application requirements while retaining a sound microstructure with high hardness.

The yield stresses calculated from the hardness values are very high for a Fe_3Al alloy. A low value of yield strength for FAS alloy (annealed condition) is approximately 250 MPa, whereas one of the highest values reported, for material prepared via reaction sintering, is 884 MPa.[17] The calculated values for coatings sprayed at 570 and 630 m/s exceed 900 MPa. Although the magnitude of yield stresses calculated from hardness values may not precisely match those measured directly, the high strengths are not unexpected. The coatings have a complex microstructure with many fine oxides, prior particle boundaries, and high dislocation densities. It is interesting to note that the hardness is not substantially lowered after heating at 800 °C and still increases with particle velocity, although the dislocation densities after heating are low and roughly equal for the three conditions. This indicates that other microstructural features, also dependent on particle velocity, contribute significantly to hardening. One example is the density of oxide stringers, which appears to increase with particle velocity.

The residual stresses present in the coatings are significantly less than the calculated yield strengths and are therefore not expected to correspond to plastic deformation. The residual stresses in the 304 stainless steel substrate, also predicted by elastic analysis of curvature, only significantly exceed the annealed yield strength in the case of the 630 m/s coating (at the coating-substrate interface), so the assumption of linear elastic behavior in curvature calculations is expected to be essentially valid.

As mentioned above, the higher kinetic energy of the spray particles is reflected in the coating microstructures. The unmelted particles have a more flattened, deformed shape in the coating produced at 630 m/s and there are fewer unmelted particles. Higher kinetic energy may reduce the fraction of unmelted particles observed by so severely deforming borderline, semisolid particles that they are not recognized as unmelted. The oxide stringers are more compressed and the overall coating thickness is less (the reduction in thickness is likely due to "splashing" of liquid particles upon impact[25]). There is no significant change in the porosity content, since even coatings produced at the lowest velocity show very little porosity.

There is no discernable effect of the measured differences in average particle temperatures on the coating microstructure or residual stresses. A higher temperature was measured for the 340 kPa chamber pressure (1732 °C), whereas lower values were measured for the other two pressures (1445 and 1592 °C for 170 and 620 kPa, respectively). Other studies have shown that particle temperature is relatively independent of chamber pressure, but rather depends more on the equivalence ratio or the point of injection into the HVOF gas stream.[13,25] The measured temperature differences in the current study may not in fact be highly significant, however, because a 5% measurement uncertainty corresponds to approximately 100 °C at these temperatures, and an intrinsic scatter in average particle temperatures of approximately 200 °C has been observed for this system.[13]

The measured values of the particle temperatures exceed the melting temperature of the Fe_3Al alloy (approximately 1540 °C[17]) for the two higher chamber pressures, but unmelted particles are readily discerned in all of the coating microstructures. The discrepancy between the measured particle temperatures and that indicated by the coating microstructure may result from burning of the aluminum component of the alloy on the particle surfaces during spraying in air. The heat and radiation emitted by the rapid surface oxidation can give rise to anomalously high pyrometer temperature readings.

As expected, heating into the B2 phase field at 800 °C for about an hour during CTE testing causes recrystallization and a corresponding reduction in dislocation density and residual stress. The dislocation density decreases by about an order of magnitude; values for all coatings are approximately 4×10^{10} cm^{-2}, still somewhat higher than typical for fully annealed metals.[24] The reductions in residual stress are shown by the shifts in the (211) peaks before and after heating (Table 7). Peak positions more closely match powder values after heating. However, as noted above, the hardness did not significantly decrease following exposure.

The agreement between the various residual stress measurements was generally very good, with some exceptions. The curvature measurements provide an average, macroscopic indication of the stress state in the coating, whereas the x-ray measurements sample the microscopic lattice strains near the analyzed surface. Both measurements indicate increasing compressive residual stress with increasing particle velocity. The magnitudes of the stresses are similar, 0-100 MPa for the 390 m/s coating, about −200 MPa for the 570 m/s coating, and about

−450 MPa for the 630 m/s coating. An ideal comparison between the two measurements would account for the removal of material during polishing of the coatings prior to x-ray analysis, but the error due to neglecting this factor is believed to be comparable to that introduced by other assumptions in the analysis. The good agreement supports the assumption of elastic behavior in the curvature measurements.

The third measure of residual stress, the change in peak position after annealing at 800 °C, indicates uniformly higher stress levels than the curvature and two-tilt XRD measurements, although the trends are similar. The source of the discrepancy may lie in the fact that the calculation of stress from the change in peak position assumes that the sole source of peak shift is the relaxation of in-plane stresses, which may be incorrect. Recrystallization processes, i.e., alleviation of local microstrains, may also cause reductions in average lattice plane spacing. Because of the assumptions required to interpret the peak shifts, the curvature and two-tilt x-ray measurements are believed to represent more accurate residual stress values.

4.2 CTE

The mean CTE of the coatings measured with x-rays in the as-sprayed condition are clearly affected by the state of residual stress present at room temperature, as demonstrated by the difference between CTE values obtained at 800 °C for heating and cooling (Fig. 3). The CTE values in the heating case are calculated using a room-temperature lattice spacing with residual strain, and for 600 and 800 °C, a strain-free spacing at temperature. Because the difference between these spacings is less than if a strain-free room temperature value was used, lower CTE values are obtained. This source of error is reflected in the ordering of CTE at 600 and 800 °C according to room-temperature residual stress levels—the lowest CTE values are obtained for samples with the highest residual stresses. The error is minimized when the relatively strain-free spacing after heating is used to calculate the cooling CTE values. In this case, there is little difference between the different particle velocities and all values more closely approximate the powder and literature values, although they do not match exactly.

The CTE for the Fe_3Al coating, however, is still less than that for powder and from the literature, even after alleviating residual stresses, as shown by the data obtained for the 630 m/s coating during a second measurement. In this case, the sample is in an annealed condition, with a strain-free room temperature lattice spacing, but the mean CTE values are still approximately 3 ppm/°C less than powder values. These differences are not due to constraint effects imposed by the substrate, because the CTE values for the Fe_3Al coating and the 304 stainless steel are very similar over the temperature range 200-800 °C (the mean CTE for 304 stainless steel is reported to be 17.5 ppm/°C at 200 °C and 19.1 ppm/°C at 800 °C[26]), but may arise from the unique microstructural features of the coating, e.g., the presence of oxide inclusions and the alignment of prior particle boundaries in the plane of the coating. The existence of fundamental differences indicates that it may not be appropriate to use bulk values to predict coating behavior under thermal cycling conditions.

The apparent reduction in mean CTE at 400 °C is currently unexplained. It was originally suspected that $D0_3$ ordering at this temperature may result in a small lattice contraction, but no $D0_3$ order was detected (by x-ray examination of the (111) $D0_3$ superlattice peak) after the approximate 1 h time required for CTE measurement.

5. Conclusions

The microstructure, residual stress, and hardness present in HVOF thermally sprayed Fe_3Al coatings were found to be strongly dependent on the HVOF particle velocity. Higher velocities give rise to increasing compressive residual stresses due to an increased peening effect. Residual stresses vary from nearly zero for coatings prepared at 390 m/s to approximately −450 MPa for coatings prepared at 630 m/s. Good agreement was found between residual stresses measured using XRD and those calculated from coupon curvature. X-ray line broadening analyses reveal a corresponding increase in the extent of cold work present in the coating, manifest as a decrease in crystallite size and increase in microstrain. The increase in cold work is also manifest in increasing microhardness with particle velocity. Yield stresses calculated from the microhardness values are high for Fe_3Al alloys, ranging from 610-1180 MPa. The microstructures of coatings prepared at higher velocities show more signs of deformation and fewer unmelted particles.

The mean CTE values obtained using x-ray analysis for as-sprayed coatings are significantly lower than those for powder and bulk alloy, primarily due to the presence of residual stresses at low temperature. The mean CTE values for an annealed coating more closely matched the powder data, but were still slightly lower.

Acknowledgments

The authors would like to acknowledge the assistance of D.C. Haggard with preparation of coatings and T.C. Morris with metallography. This work is supported by the U.S. Department of Energy, Office of Fossil Energy, under DOE Idaho Operations Office contract DE-AC07-99ID13727.

References

1. C.G. McKamey, J.H. DeVan, P.F. Tortorelli, and V.K. Sikka: "A Review of Recent Developments on Fe3Al-Based Alloys," *J. Mater. Res.*, 1991, *6*(8), pp. 1779-805.
2. N.S. Stoloff: "Iron Aluminides: Present Status and Future Prospects," *Mater. Sci. Eng. A*, 1998, *A258*, pp. 1-14.
3. U. Prakash, R.A. Buckley, H. Jones, and C.M. Sellars: "Structure and Properties of Ordered Intermetallics Based on the Fe-Al System," *Iron and Steel Institute of Japan International,* (*ISIJ*) 1991, *31*(10), pp. 1113-26.
4. P.F. Tortorelli and J.H. DeVan: "Behavior of Iron Aluminides in Oxidizing and Oxidizing/Sufidizing Environments," *Mater. Sci. Eng. A*, 1992, *A153*, pp. 573-77.
5. P.F. Tortorelli and K. Natesan: "Critical Factors Affecting the High-Temperature Corrosion Performance of Iron Aluminides," *Mater. Sci. Eng. A*, 1998, *A258*, pp. 115-25.
6. R.N. Wright, J.R. Fincke, W.D. Swank, D.C. Haggard, and C.R. Clark: "The Influence of Process Parameters on the Microstructure and Properties of Fe3Al Based Coatings" in *Elevated Temperature Coatings: Science and Technology I*, N.B. Dahortre, J.M. Hampikian, and J.J. Stiglich, ed., TMS, Warrendale, PA, 1995, pp. 157-66.
7. T. Grosdidier, H.L. Liao, and A. Tidu: "X-Rays and TEM Characterization of Nanocrystalline Iron Aluminide Coatings Prepared by HVOF Thermal Spraying" in *Thermal Spray: Surface Engineering Via Applied*

Research, C.C. Berndt, ed., ASM International, Materials Park, OH, 2000, pp. 1341-44.
8. T.W. Clyne and S.C. Gill: "Residual Stresses in Thermal Spray Coatings and Their Effect on Interfacial Adhesion: A Review of Recent Work," *J. Therm. Spray Technol.*, 1996, *5*(4), pp. 401-18.
9. S.C. Gill and T.W. Clyne: "Stress Distributions and Material Response in Thermal Spraying of Metallic and Ceramic Deposits," *Metall. Trans. B*, 1990, *21B*, pp. 377-85.
10. S. Kuroda: "Properties and Characterization of Thermal Sprayed Coatings—a Review of Recent Research Progress" in *Thermal Spray: Meeting the Challenges of the 21st Century*, C. Coddet, ed., ASM International, Materials Park, OH, 1998, pp. 539-50.
11. S. Kuroda, Y. Tashiro, H. Yumoto, S. Taira, and H. Fukanuma: "Peening Action and Residual Stresses in HVOF Thermal Spraying of 316L Stainless Steel" in *Thermal Spray: Meeting the Challenges of the 21st Century*, C. Coddet, ed., ASM International, Materials Park, OH, 1998, pp. 569-74.
12. W.D. Swank, J.R. Fincke, D.C. Haggard, and G. Irons: "HVOF Gas Flow Field Characteristics" in *Thermal Spray Industrial Applications*, C.C. Berndt and S. Sampath, ed., ASM International, Materials Park, OH, 1994, pp. 307-12.
13. W.D. Swank, J.R. Fincke, D.C. Haggard, G. Irons, and R. Bullock: "HVOF Particle Flow Field Characteristics" in *Thermal Spray Industrial Applications*, C.C. Berndt and S. Sampath, ed., ASM International, Materials Park, OH, 1994, pp. 319-24.
14. W.D. Swank, R.A. Gavalya, J.K. Wright, and R.N. Wright: "Residual Stress Determination From a Laser-Based Curvature Measurement" in *Thermal Spray: Surface Engineering Via Applied Research*, C.C. Berndt, ed., ASM International, Materials Park, OH, 2000, pp. 363-69.
15. C.H. Hsueh and A.G. Evans: "Residual Stresses in Metal/Ceramic Bonded Strips," *J. Am. Ceram. Soc.*, 1985, *68*(5), pp. 241-48.
16. S.H. Crandall, N.C. Dahl, and T.J. Lardner: *An Introduction to the Mechanics of Solids*, 2nd ed., McGraw-Hill, New York, 1978.
17. J.H. Schneibel: "Selected Properties of Iron Aluminides" in *Processing, Properties, and Applications of Iron Aluminides*, J.H. Schneibel and M.A. Crimp, ed., TMS, Warrendale, PA, 1994, pp. 329-42.
18. B.E. Warren: "X-Ray Studies of Deformed Metals," *Prog. Metal Phys.*, 1959, *8*, pp. 147-202.
19. I.C. Noyan and J.B. Cohen: *Residual Stress—Measurement by Diffraction and Interpretation*, Springer-Verlag, New York, 1987.
20. B.D. Cullity: *Elements of X-Ray Diffraction*, 2nd ed., Addison-Wesley, Reading, MA, 1978.
21. G.K. Williamson and R.E. Smallman III: "Dislocation Densities in Some Annealed and Cold-Worked Metals From Measurements on the X-Ray Debye-Scherrer Spectrum," *Philos. Mag.*, 1956, *1*, pp. 34-46.
22. J.R. Cahoon, W.H. Broughton, and A.R. Kutzak: "The Determination of Yield Strength From Hardness Measurements," *Metall. Trans. A*, 1971, *2*(7), pp. 1979-83.
23. G.E. Dieter: *Mechanical Metallurgy*, 3rd ed., McGraw-Hill, New York, 1986.
24. D. Hull and D.J. Bacon: *Introduction to Dislocations*, Pergamon Press, New York, 1984.
25. C.M. Hackett and G.S. Settles: "Independent Control of HVOF Particle Velocity and Temperature" in *Thermal Spray: Practical Solutions for Engineering Problems*, C.C. Berndt, ed., ASM International, Materials Park, OH, 1996, pp. 665-73.
26. S.D. Washko and G. Aggen: "Wrought Stainless Steels" in *Metals Handbook*, 10th ed., ASM International, Materials Park, OH, 1990, p. 871.